Single cell respirometry and 3D cytometry of MCF-10A and MDA-MB-231 cells

Vivek Nandakumar, Laimonas Kelbauskas, Shashanka Ashili, Patti Senechal,

Roger H. Johnson, and Deirdre R. Meldrum

Center for Biosignatures Discovery Automation, Biodesign Institute, Tempe, Arizona

Project 3 ASU PS-OC

Abstract

We apply two single cell methods to perform comparative studies on the UCSF cell lines: cell respirometry, in which we measure the cells' respiration rates; and 3D cytomorphometry, in which we quantify the 3D structure of fixed cells stained with Hematoxylin and Eosin (H&E). We measured oxygen consumption rates (OCR) of individual live cells in hermetically sealed microchambers using extracellular optical sensors. We found significant cell-to-cell variations in oxygen consumption rates within the same cell type and marked differences in OCR between the non-tumorigenic (high OCR) and the metastatic (low OCR) cell types. To quantify cell morphology, we imaged H&E-stained cells using single-cell optical absorption computed tomography and extracted quantitative morphological descriptors or features from the volumetric cell images. 3D cytometry revealed several interesting trends in cellular and nuclear morphology and in coarse heterochromatin texture between the two lines. Using our quantitative methods, we plan to develop biosignatures to robustly distinguish between the two cells types based on their structure and respiration phenotype. We plan to correlate observed differences in OCR values to the alterations in the nuclear morphology and high-order chromatin organization to explore potential structure-function relationships in the two cell types.

Introduction

Variations in cell physiology and structure are important consequences and indicators of malignancy. Genomic changes are known to mediate alterations in cell physiology and structure. However, detailed links between these key factors in cell functioning are not well understood.

Changes in the cell architecture were shown to be associated with transcription repression and induction of hundreds of genes in human mammary epithelial cells (*1*). Modulation of gene expression may be related to changes in nuclear morphology, which can cause dislocations and distortions in chromatin organization, alterations in DNA wrapping and accessibility to transcription and chromatin remodeling factors. In mammalian cells chromatin localization and orientation within the nucleus play an essential role in expression and silencing of certain genes (*2*). A recent study has indicated a direct role of chromatin structure in acute drug resistance in cancer cells (*3*).

The oxygen consumption phenotype is important as it directly reflects cell metabolism and energy production. Because of its strong role in many cellular signaling and regulation processes, changes in oxygen consumption represent a sensitive indicator for physiological alterations within the cell. Thus, characterization of oxygen consumption rates of individual cells permits sensitive monitoring of alterations in cell metabolic state under physiological and pathological conditions.

We present experimental findings of a comparative study focused on two aspects of the cell structure-function relationship in the two cell lines: a) characterization of nuclear morphology and chromatin distribution using optical absorption computed tomography and b) oxygen consumption phenotype characterization at the single-cell level. From our preliminary data, we find notable distinguishing trends in nuclear structure and higher-order chromatin distribution between MCF-10A and MDA-MB-231 cells. The MCF-10A cells exhibited faster oxygen consumption rates by a factor of ~2 as compared to MDA-MB-231 cells. These findings indicate the importance of nuclear structure-function relationships in the context of cancer.

Materials and methods

Cell culture: MCF-10A and MDA-MB-231 cell lines were cultured according to prescribed PS-OC protocols. Prior to experimentation, cells were cultured in a 75-cm flask to approximately 80% confluence, at which time they were trypsinized and centrifuged at 900 rpm for 3 minutes and resuspended in 3 ml of appropriate medium. The cell viability was determined to be at least 95% using the Countess® cell counter.

Cell Respirometry: We have optimized and implemented experimental protocols for reliable and fast cell manipulation and oxygen consumption measurements. Based on the protocols, we have conducted a series of experiments focusing on determination of oxygen consumption phenotype at the single-cell level. Respirometry experiments at the single-cell level were conducted by means of measuring phosphorescence intensity of an extracellular oxygen sensor as a function of time in sealed microchambers containing individual cells. All cells were grown in corresponding cell media and were untreated otherwise. To assess the cells' respiration rates, we load individual cells into microwell arrays and incubate them for 16 to 22 hours prior to experiment. Then we hermetically seal the arrays of microwells with corresponding arrays of microlids. Extracellular platinum porphyrin sensors, deposited in the microwell lids, are monitored and read out in order to determine the cell respiration rate. The sensor luminescence signal was acquired by means of bright field illumination with a deep-blue LED (λ_{max}=396 nm) and a high-sensitivity cooled EMCCD camera as a detector.

Tomographic imaging and 3D morphometry

Sample preparation

To enable tomographic imaging of cells, we stain them with H&E for transmission absorption imaging. Hematoxylin is an acidophilic dye that emphasizes the nucleus while Eosin is a basophilic dye that stains the cytoplasm.

We fixed the cells with CytoLyt (Cytyc, Malborough, MA) and smeared them onto a microscope glass slide (VWR, West Chester, PA) coated with 0.01% Poly-L-Lysine (PLL) (Sigma Aldrich, St. Louis, MO). Prior to coating with PLL the slide was washed with 2% Neutrad detergent (Fisher Scientific, Fair Lawn, NJ) and then rinsed thoroughly with de-ionized water. We stained the cells for a few minutes (cell line dependent) in aqueous 6.25% w/w Gill's hematoxylin (Electron Microscopy Sciences, Hatfield, PA) solution, then counter-stained in bluing reagent (Fisher Scientific, Fair Lawn, NJ) for 30 seconds after washing thrice with filtered tap water. After an additional three washes with filtered tap water, we stained the cells with 1% Eosin (Electron Miscroscopy Sciences, Hatfield, PA). We then subjected the cells to dehydration through an ethanol series (50%, 95%, and 100%) and two washes with 100% xylene. Lastly, we embedded the stained cells into a special carrier gel (Smart Gel, Nye Lubricants, Fairhaven, MA) and loaded the resulting cell-gel suspension into a glass syringe (Hamilton, Reno, NV) for tomographic imaging.Since proper staining is highly dependent on experimental conditions (including pH of the water used), we carried out multiple trials to optimize the concentrations of reagents and durations of protocol steps.

Tomographic imaging

We performed optical tomographic imaging of stained, individual cells using a computed tomography (CT) instrument (VisionGate, Gig Harbor, WA). The cell CT instrument provides isotropic spatial resolution of ~350 nm. We imaged the cells sequentially by flowing the carrier gel through a rotating glass capillary. For each cell, we generated a volumetric image by acquiring 500 projection images taken at angular

intervals of 0.72 degrees around the cell and subjecting these projection images to mathematical reconstruction algorithms. Prior to reconstruction, we de-noised and aligned the projection images to remove pattern noise artifacts and to compensate for mechanical jitter and runout of the capillary, respectively. We imaged one hundred cells from each cell line and used the generated volumetric images for morphometric analysis.

3D morphometry

We quantified cell and nuclear structure with robust 3D image processing algorithms applied to the cell image data. We denoised the image, segmented the volumes of interest (VOIs) including the cell, the nucleus, nuclear compartments and the nuclear DNA, and computed morphological and textural descriptors (or features) from the segmented VOIs. We computed a total of forty features that quantified the morphology of objects within the VOIs and the texture of chromatin. Specifics of the feature extraction and the list of extracted features are detailed in Table 1.

To achieve high throughput analysis we used Matlab software (Mathworks, Natick, MA) to automate the 3D image processing sequence. We used Origin 8.0 software (OriginLab, Northampton, MA) to statistically characterize distributions of the extracted 3D nuclear morphometric feature data and to compute histograms revealing quantitative differences between corresponding features in the two cell lines.

Results

Figure 1 shows representative volume renderings of reconstructed 3D cell CT images of MCF-10A and MDA-MB-231 cells. The renderings were created using VolView software (Kitware, Clifton Park, NY). Histograms of select morphological and textural features are shown in Figures 2, 3. Figure 4 depicts the oxygen consumption of MCF-10A and MDA-MD-231 cells over time. Comparative results of oxygen consumption rates between the two cell lines are shown in Figure 5.

We observe the following trends based on our preliminary data.

MCF-10A and MDA-MB-231 cells exhibit different oxygen consumption profiles at the single-cell level

Utilizing the custom-developed technology for measurements of the oxygen consumption phenotype at the single-cell level, oxygen consumption rates (OCRs) of cell from both cell lines were determined. Individual cells were loaded into microwells and incubated for 16-22 hrs prior to experiments. OCRs were measured using extracellular optical sensor deposited in the top part of the microchamber containing a single cell. During the experiment oxygen concentration in the sealed microchambers was measured every 5 seconds. The experiment was continued until O_2 concentration decreased to 0 ppm within the measurement error. In both cell lines a linear decrease in oxygen concentration as a function of time was observed (Fig. 4a, b). The OCRs results are summarized in Fig. 5. To allow a better comparison between the two cell lines the numbers of cells in each bin of the histogram were normalized against the total number of measured cell in the corresponding cell line. The total numbers of the measured MCF-10A and MDA-MB-231 cells are 12 and 39, respectively. On average, we observe slower respiration rates in MDA-MB-231 compared to MCF-10A cells by a factor of ~2. The mean OCR value determined for MDA-MB-231 cells is 2.13±0.31, whereas the OCR value for MCF-10A is 3.71±0.87. Keeping in mind that the cells used for the measurements were not synchronized and, thus, represent different stages in the cell cycle, the observed difference indicates that on average MDA-MB-231 cells consume oxygen more slowly that MCF-10A cells. The amount of data collected precludes any definitive conclusions regarding the differences in OCR observed. More data is being collected to improve the statistical significance of the obtained results.

The significantly lower OCR measured in MDA-MB-231 cells compared to MCF-10A cells implies that MDA-MB-231 cells have less pronounced oxidative phosphorylation pathway. It is known that cancer cells tend to undergo anaerobic glycolysis even when under normoxic conditions (the Warburg effect). It is likely that in MDA-MB-231 cells a substantial amount of the energy required for growth and proliferation is produced by the glycolytic pathway.

MCF-10A cells exhibit diverse morphologies

We observe that the MCF-10A cell line exhibits a wide range of morphologies. This is evidenced in Figure 2 by the notably non-gaussian statistical distributions of several morphological features. Cell cycle could be a factor contributing to the observed morphological variations, but FACS-based cell sorting experiments prior to cell fixation indicate that a majority of the cultured cells were in G1 phase.

MCF-10A and MDA-MB-231 nuclei are not always spherical

This is evidenced from the distribution of the 'nuclear compactness' feature in Figure 2(d). Nuclear compactness is the ratio of the cube of the surface area to the square of the volume; a large value of this metric is associated with departure from sphericity. For example, the MDA-MB-231 cell in the bottom row of Figure 1 has a much higher value of this metric than the near-spherical MCF-10a cell depicted in the top row.

Reversal of morphological trends associated with malignancy

The established cytopathological indicators of morphological changes associated with malignancy are increases in parameters such as nuclear volume, nucleus-to-cytoplasm ratio (NC ratio), number of nucleoli, and margination of the nucleoli towards the nuclear periphery. However, in Figure 2, we observe that these traits are exhibited by the non-tumorigenic MCF-10A cell line. The similarity in morphological feature distributions between the two cell lines is noteworthy and merits further investigation.

A similar trend is observed in textural variations between the two cell lines. In Figure 3 (b-e), we observe that the MCF-10A cells exhibit more variations in chromatin organization and steeper, more abrupt transitions between chromatin densities.

Discussion

Our inferences are based on preliminary data. Better statistics will result from the accumulation of more data which will be available in by fall of 2010. We plan to assess the effect of cell cycle on our measurements by means of using sorted (synchronized) cells. A true mammary epithelial control cell line would be a valuable addition to the cell line paper.

References

(1)   Alcaraz, J., Xu, R., Mori, H., Nelson, C. M., Mroue, R., Spencer, V. A., Brownfield, D., Radisky, D. C., Bustamante, C., and Bissell, M. J. (2008) Laminin and biomimetic extracellular elasticity enhance functional differentiation in mammary epithelia. *Embo Journal 27*, 2829-2838.

(2)   Finlan, L. E., Sproul, D., Thomson, I., Boyle, S., Kerr, E., Perry, P., Ylstra, B., Chubb, J. R., and Bickmore, W. A. (2008) Recruitment to the nuclear periphery can alter expression of genes in human cells. *Plos Genetics 4*, -.

(3)   Sharma, S. V., Lee, D. Y., Li, B. H., Quinlan, M. P., Takahashi, F., Maheswaran, S., McDermott, U., Azizian, N., Zou, L., Fischbach, M. A., Wong, K. K., Brandstetter, K., Wittner, B., Ramaswamy, S.,
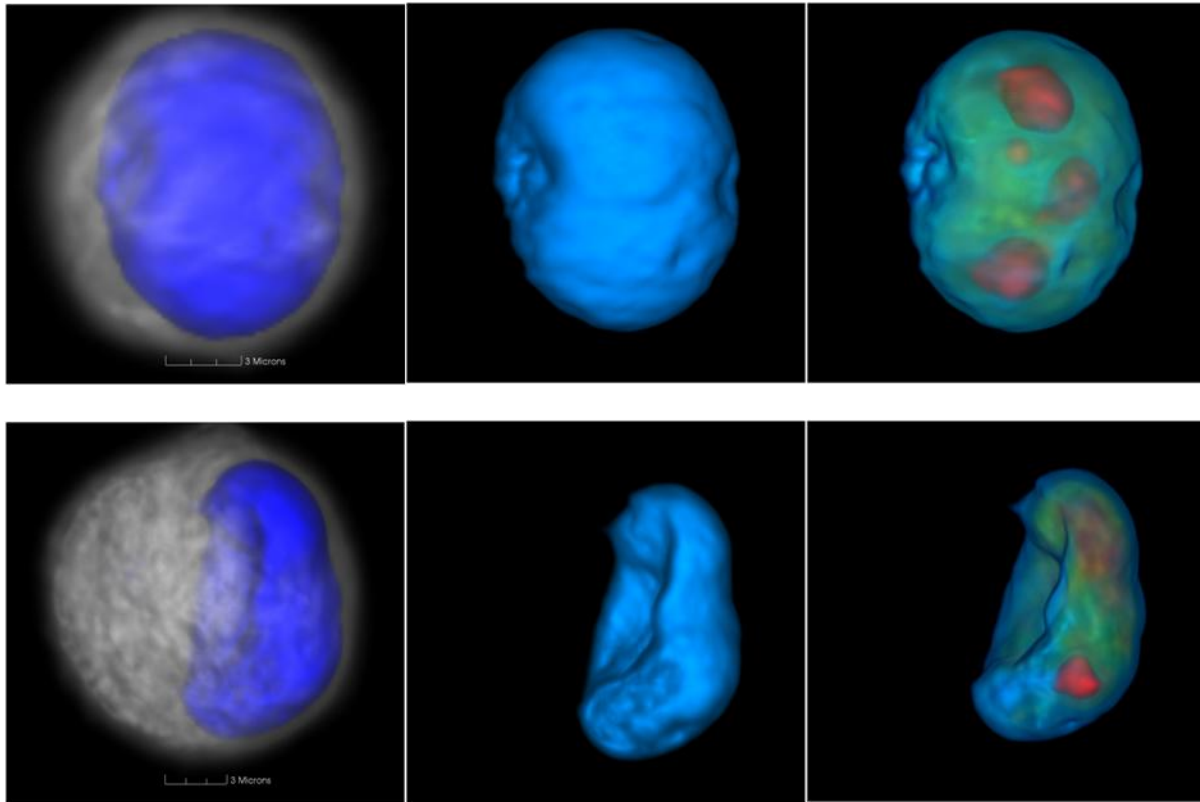
Classon, M., and Settleman, J. (2010) A Chromatin-Mediated Reversible Drug-Tolerant State in Cancer Cell Subpopulations. *Cell 141*, 69-80.

Table 1: Morphometric features

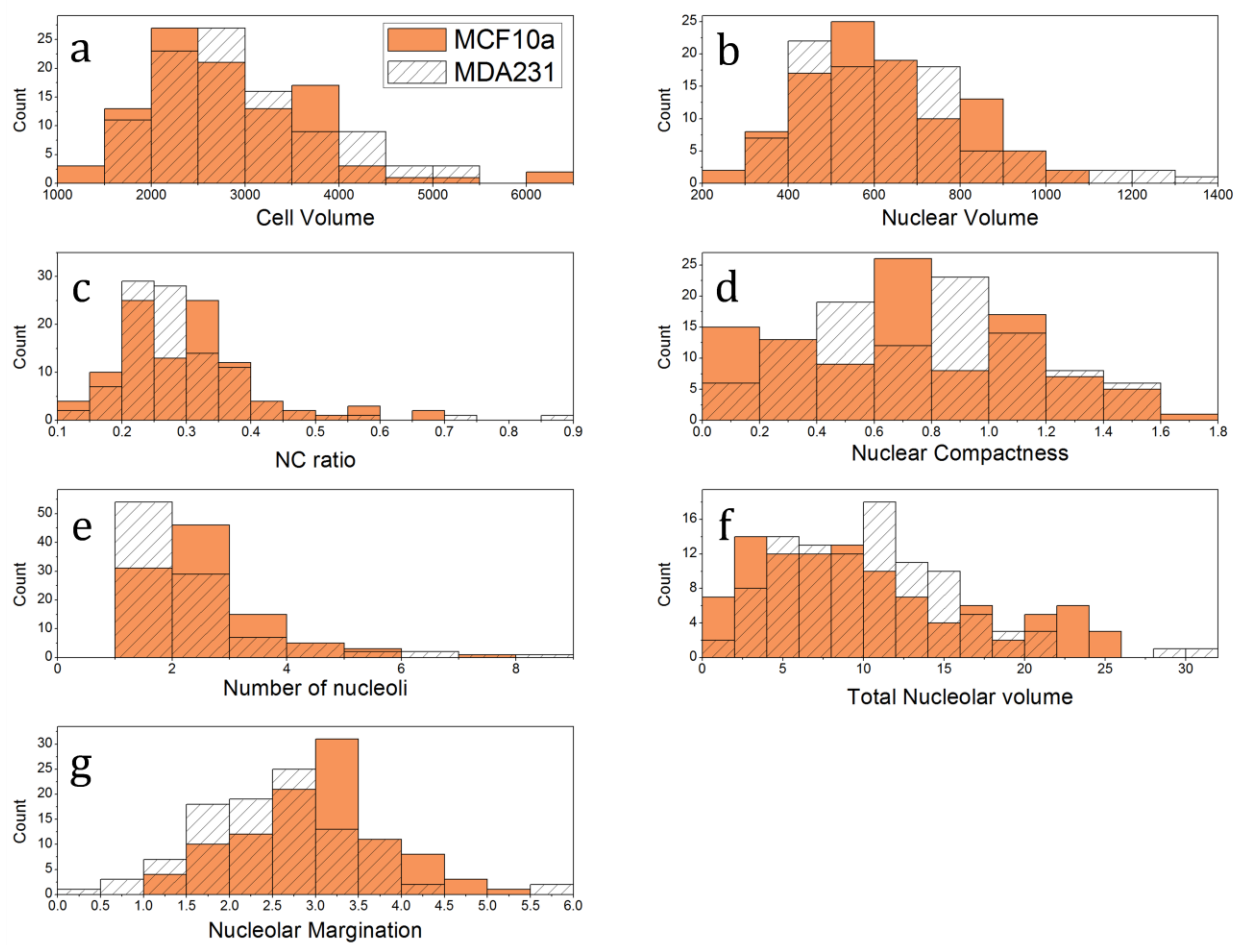| Feature type	Feature specifics*
Morphological (7)	cell volume, nuclear volume, nucleus to cytoplasm volume ratio, number of nucleoli, total nucleolar volume, mean nucleolar volume, mean nucleolar proximity (to nucleus center)
Descriptive texture (5)	integrated optical density, mean optical density, variance in optical density, skew in optical density, kurtosis in optical density
Discrete texture (24)	number of objects in low, medium and high DNA condensation states (3), volume fraction of each condensation state (3), optical density fraction of each condensation state (3), average extinction ratio of each condensation state (3), compactness of each condensation state (4), average distance of voxels in each condensation state from nucleus center (4), average distance of center of each condensation state from the nucleus center (4)
Markovian texture (4)	energy, contrast, correlation, homogeneity

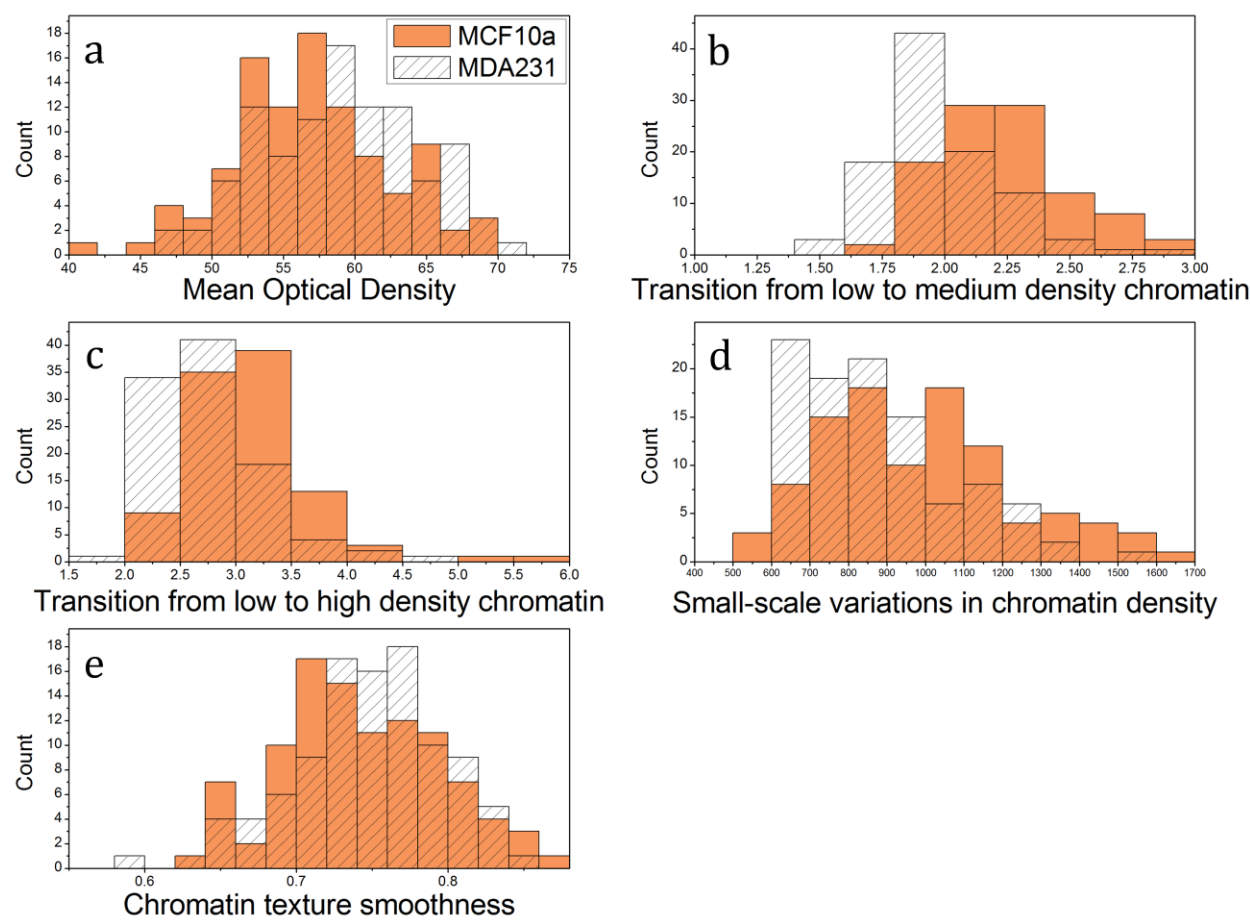* Numbers in parentheses indicate the number of features of a given type

Figure 1

Volume renderings of MCF-10A (top) and MDA-MB-231 (bottom) cells. Left images depict cell (in gray) and nuclear (in blue) surfaces, middle images illustrate the nuclear surface, and right images are transparencies that show the nuclear interior. Increasing nuclear DNA density is color coded from green to red. The most prominent feature in the MDA-MB-231 cells is the highly irregular shape of the nucleus.
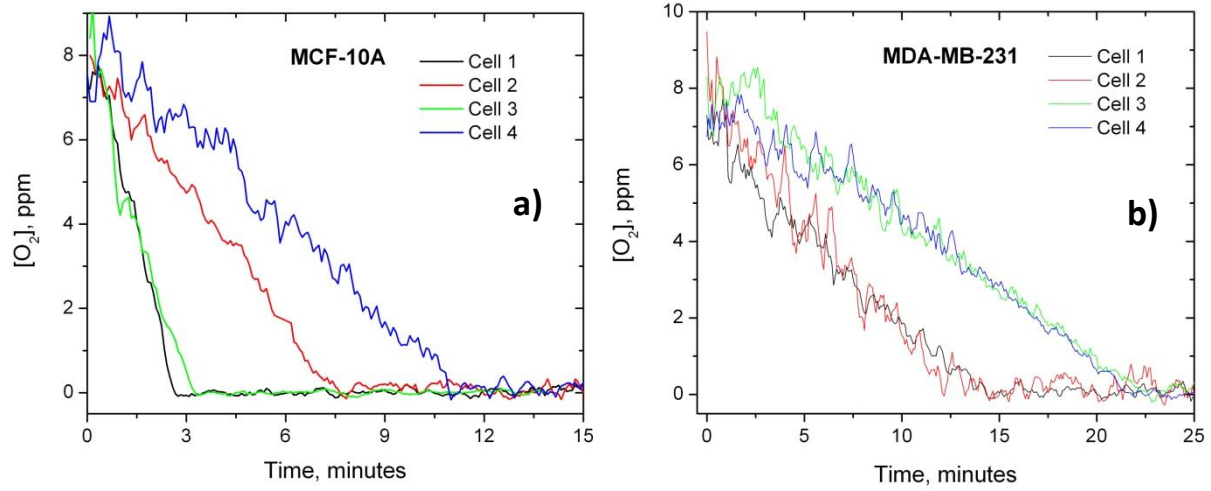
Figure 2

Histograms for select 3D morphological features reveal structural characteristics of MCF-10A and MDA-MB-231 cell lines (N = 100 cells per line). The distributions indicate a wide variation in structure within a cell line. A second notable observation is the similarity in morphological traits between the two cell lines.
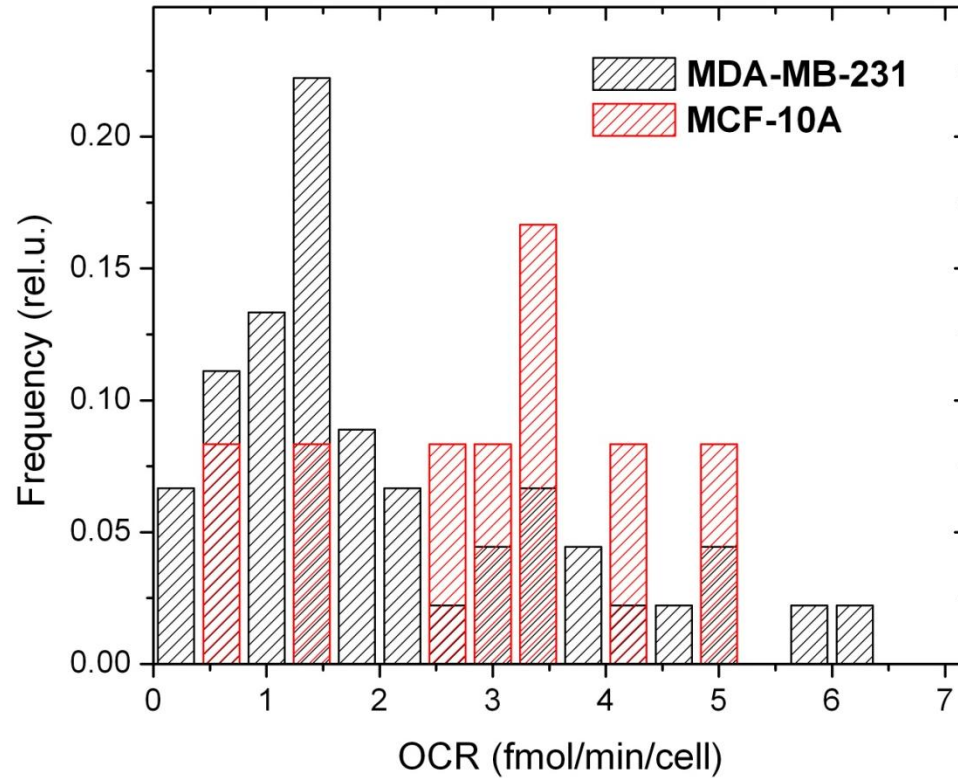
Figure 3

Histograms for select 3D textural features indicate variational trends in chromatin distribution between the two cell lines. Abnormal cells are characterized by (a) higher-density DNA and (b-e) smoother transitions between different densities of chromatin.

Figure 4

Oxygen consumption rates of individual MCF-10A (a) and MDA-MB-231 (b) cells measured utilizing the single-cell respiration phenotype characterization platform. O_2 concentration in hermetically sealed microchambers decreases as the cell respires. Data points were obtained every 5 seconds. Each curve in the panels represents respiration time course of a corresponding single cell. A sliding smoothing algorithm with 5-point window was applied to the data. Cells from both cell lines show linear or close-to-linear consumption of oxygen as a function of time. MDA-MB-231 cells exhibit slower respiration rates than MCF-10A cells.

Figure 5

A summary of the single-cell respirometry results obtained with MDA-MB-231 and MCF-10A cells. The OCR values were calculated by fitting the oxygen consumption time courses to a linear regression model. To allow a better comparison between the two cell lines, the numbers of cells in each bin of the histogram were normalized against the total number of the corresponding measured cells. On average, MCF-10A cells exhibit higher respiration rates by a factor of ~2 as compared to MDA-MB-231 cells.